

https://dspace.org/

Thermophoretic particle deposition in a mixed convective bioconvection nanofluid with thermal radiation and chemical reaction over an exponential stretching sheet

R Baithalu; Folarin Oluwaseun; Titilayo Agbaje; S Mishra; S Panda

https://hdl.handle.net/10539/47587
WOS

Downloaded from a DSpace repository. https://dspace.org/

Multiscale and Multidisciplinary Modeling, Experiments and Design (2025) 8:220
https://doi.org/10.1007/s41939-025-00805-3

ORIGINAL PAPER

Thermophoretic particle deposition in a mixed convective bioconvection nanofluid with thermal radiation and chemical reaction over an exponential stretching sheet

Rupa Baithalu[1] · Folarin Oluwaseun[2] · Titilayo M. Agbaje[3] · S. R. Mishra[1] · Subhajit Panda[4]

Received: 18 December 2024 / Accepted: 15 February 2025 / Published online: 9 March 2025
© The Author(s), under exclusive licence to Springer Nature Switzerland AG 2025

Abstract
Thermophoretic particle deposition in a mixed convective bioconvection nanofluid across an exponential stretching sheet embedding within a porous matrix is presented in this article. The analysis accounts for the thermal radiation and chemical reactions that are useful in various engineering and biological applications. The bioconvection for the movement of motile microorganisms significantly enriches heat and solutal transport phenomena. The proposed dimensional governing equations are re-framed to non-dimensional form by utilizing similarity rules which involve diversified factors. The nonlinear coupled transformed set of equations is handled numerically for the employment of the "*spectral quasilinearization method*" (SQLM) ensuring high accuracy and computational efficiency. The physical behaviour of the pertinent factors involved in the phenomena are discussed and presented in the discussion section. The results are compared with the existing literature showing good agreement and also provide the convergence of proposed methodology. The study reveals a promising application in biotechnological processes i.e., targeted drug delivery, environmental systems involving permeability i.e. groundwater remediation and filtration processes, industrial processes like polymer extrusion, etc. where the control of particle deposition are required.

Keywords Bioconvection · Exponential stretching sheet · Thermal radiation · Thermophoretic deposition · Spectral quasilinearization method

✉ S. R. Mishra
satyaranjan_mshr@yahoo.co.in

Rupa Baithalu
rupadhananjaygarnaik@gmail.com

Folarin Oluwaseun
folarino987@yahoo.com

Titilayo M. Agbaje
titilayoagbaje@gmail.com

Subhajit Panda
spanda.math@gmail.com

[1] Department of Mathematics, Siksha 'O' Anusandhan Deemed to be University, Bhubaneswar, Odisha 751030, India

[2] School of Mathematics, Statistics, and Computer Science, University of the KwaZulu-Natal, Private Bag X01, Scottsville 3209, Pietermaritzburg, South Africa

[3] School of Computer Science and Applied Mathematics, University of the Witwatersrand, Private Bag 3, Johannesburg 2050, Braamfontein, South Africa

[4] Centre for Data Science, Department of Computer Science and Engineering, Siksha 'O' Anusandhan Deemed to be University, Bhubaneswar, Odisha 751030, India

1 Introduction

Bioconvection is an intriguing process that arises from the collective motion of microorganisms within fluid systems, resulting in intricate flow dynamics. This phenomenon is largely driven by the self-directed movement of organisms like bacteria and algae. Bioconvection significantly impacts both natural ecosystems and engineered systems, affecting nutrient cycling, ecological relationships, and the clustering of biomass in aquatic settings. Aboel-Magd et al. (2024) reported the characteristic of bioconvection on the heat transport phenomena of Casson nanofluid flow through a disk. As a novel approach the role of binary chemical reaction including gyrotactic microorganisms have been discussed in their investigation with complex design. The proposed model equipped with various flow properties corresponds to their standard non-dimensional form are solve by employing shooting based numerical technique and they have used bvp4c solver in MATLAB. Ullah et al. (2023) presented a bioconvective motion of Casson nanofluid for the interaction of buoyant forces over an extending surface and they

have introduced the impact of external heat source vis-à-vis the imposition of dissipation that energies the heat transport phenomenon. The physical significance of the characterizing factors is interpreted by utilizing the numerical simulation of the flow profile. An interesting feature is that the shear rate and motion density increase with the increase of the Rayleigh number of biological propagation. The electrically conducting bioconvective nanofluid flow over diversified geometries is conducted by Choudhary et al. (2024) incorporating the impact of motile microorganisms. They have projected a comparative analysis by considering the flow through a wedge, flat plate, considering a stagnation point flow. The focus of the study is to show the impact of bimolecular reaction along with the role of cross-diffusion in melting condition. The built-in function "bvp4c" solver in MATLAB is used to handle the governing transformed equations numerically in association with the impact of several factors in their respective ranges. Rehman et al. (2024) deployed the transport of heat characteristic considering a mixed convective flow associated with viscous liquid within a vertical cylinder executing the impact of swimming microorganisms. Moreover, the integration of nanofluid and microorganism in several technical innovations as well as in engineering particularly in heat transfer analysis is proposed by Faizan et al. (2024). They have highlighted their study for the categorical behavior of motile microorganism considering a conducting non-Newtonian fluid for the introduction of radiative heat and reactive species. For the improvement of their model the interaction of external heart source/sink for Cattaneo-Christov heat flux theory is also considered. The mathematical model proposed with aforesaid phenomena are resolved numerically that embedding with various physical parameters.

In present investigation, the flow over an exponentially expanding surface presents its significant attention particularly combined with the role of radiating heat energy. For the flow behavior of the fluid within the surrounding, the role of this kind sheets presents their major impact and flow through this kind of geometries have significant applications in various engineering. However, for the overall balance of energy that enhance the improves the heat transfer mechanism, the use of thermal radiation is essential. Various properties of the thermal radiation are exhibited for its interaction over stretching surface and its distribution. Alharbi et al. (2023) explored the properties of Maxwell-Sutterby nanofluid and its heat transfer enhancement where the fluid flowing over an expanding surface. In an advance the role of activation energy and radiating heat affects the temperature of nanofluid. Furthermore, the exponential heat generation or absorption, and the influence of motile microorganisms, shows significant enhancement of the flow of bioconvection. The characteristic of Powell-Eyring liquid via an exponentially enlarging sheet is presented by Agrawal et al. (2024). They have projected the transport phenomena of nanofluid flow governed by the proposed model through an exponentially enlarging surface with the characteristic of motile microorganisms. Layek et al. (2007) proposed the heat transport properties of the flow through stagnation-point over a permeable expanding surface subjected to thermal heating. The insertion of external heat source/sink vis-à-vis the suction/injection enhances the flow properties significantly. Further, in recent studies, Loganathan and Rajan (2020) deployed the impact of magnetic dissipation and the convective heat transfer phenomena considering the significance of Williamson nanofluid where the flow past an elongating surface. Additionally, Kumar et al. (2020) also reported the development of heat transport properties are obtained by the introduction of dissipative heat and nonlinear radiation considering Williamson nanofluid flow over an expanding surface. Waseem et al. (2024) considered the circulation of polar nanofluid which is flowing past a stretching surface with the addition of radiant heat and heat sources. The inclusion presence of motile microorganisms is one of the important aspects of their study. The proposed flow past through an exponentially enlarging sheet packed with permeability enhances the features of the physical properties. In a novel approach statistical analysis is performed to execute the role of various factors affecting the flow and thermal transportation characteristics.

The solution of the transformed models is handled both analytically as well as numerical techniques. In particular several semi-analytical methods are also useful for the solution of this type of models. Out of several techniques, spectral quasilinearization method (SQLM) is one of the powerful computational techniques shows a high degree of accuracy and efficiency. Das et al. (2023) proposed an entropy analysis considering micropolar fluid flow through a vertical heated sheet where the modelled problems governed by the flow properties are solved via spectral collocation technique numerically. The computations are conducted using the "spectral quasilinearization method" (SQLM) combined with the overlapping grids approach. Further, Francis et al. (2024) presented the behavior of nanomaterials on the surface of a cone, solving the governing ODEs utilizing bvp4c solver in MATLAB. Ratha et al. (2022) examined the imposition of MHD nanomaterials containing various solid particles in a mixture of H_2O and ethylene glycol as base fluids, focusing on flow dynamics over a radially extending sheet filled with porous. They have applied the "*Differential Transform Method*" and the "*Pade-Approximant technique*" through suitable similarity transformations. Li et al. (2022) focused on the influence of a transverse magnetism with the interaction of buoyant forces considering a time-dependent nanofluid across a permeable vertical sheet. Thumma et al. (2022) imposed numerical technique in analyzing the behavior of density variations

and a non-uniform heat supplier along with sink considering Maxwell nanofluid over a stretching surface, where the solution of the model problem is presented numerically. Moreover, Mahmud et al. (2022) investigated the bioconvective microorganisms for the interaction of the Lorentz force utilizing permeable Riga surface, using a couple stress model. Baithalu et al. (2024) revealed the behavior of radiative hybrid nanomaterials in spinning geometries, such as cones and circular discs. Their study examines the influence of magnetism on the thermal and flow features of nanomaterials in these rotating systems, accounting for the mutual effects of radiation and magnetic dissipation. These findings provide critical insights for improving thermal management in advanced commercial applications. Amjad et al. (2023) analyzed the transmission of Magnetohydrodynamic (MHD) flow utilizing nanomaterials through an exponentially elastic sheet, using numerical methods to study how magnetic fields affect flow dynamics and energy transport. This investigation broadens the understanding of MHD nanofluids for various engineering applications. Hsiao (2017) focused on the flow of Carreau liquids, incorporating the effects of heat radiation and bimolecular reactions into the analysis.

Wang et al. (2025) explored a novel fusion of numerical techniques and advanced computational intelligence to analyze the behavior of cross nanofluid flow over a Riga plate within a Darcy-Forchheimer porous medium. The melting heat phenomenon in the viscous nanofluid MHD flow over a stretching sheet with variable porosity and permeability was investigated by Wang et al. (2024). The magneto-viscous nanofluid flow behavior was analyzed through the application of machine learning and statistical techniques. Abbas et al. (2024) examined the effect of viscous dissipation on the stagnation point flow of a trihybrid nanofluid in the influence of Marangoni convection and activation energy. Additionally, the study incorporates the impacts of heat generation and a magnetic field. Okasha et al. (2024) scrutinised the influence of Stefan blowing on the stagnation point flow of a hybrid nanofluid concluded a sheet embedded with gyrotactic microorganisms under local thermal non-equilibrium conditions. Elboughdiri et al. (2024) investigates the influence of Soret and Dufour effects on the three-dimensional flow of a trihybrid nanofluid (THNF) over a sheet embedded in a porous medium, considering thermal radiation and Stefan blowing effects. The analysis employs two distinct thermal conductivity models: the Hamilton-Crosser model (HCM) and the Yamada-Ota model (YOM). Mahariq et al. (2025) examined the effects of Marangoni convection and inclined magnetohydrodynamics (MHD) on the axisymmetric Darcy–Forchheimer flow of a ternary hybrid nanofluid over an infinite disk, incorporating melting processes. Janapatla et al. (2023) inspected the mixed convective flow of a nanofluid past a vertical wedge, incorporating the effects of radiation, magnetohydrodynamics (MHD), Brownian motion, and thermophoresis. The study by Alghamdi et al. (2021) delves into the radiative-convective behavior of sodium alginate-based nanofluids within a Darcy-Brinkman porous structure. Sodium alginate, a biopolymer with favorable viscosity and thermal characteristics, serves as the base fluid, providing a unique perspective on nanofluid performance. In their study, Chu et al. (2021) delve into the rheological behavior of MWCNT-TiO_2 nanoparticles dispersed in 5W40 engine oil, forming a hybrid nanofluid. The research is particularly significant as it bridges the gap between experimental investigations and predictive modeling techniques such as response surface methodology (RSM) and artificial neural networks (ANN). The authors employ an experimental approach to characterize the nanofluid' viscosity and shear-thinning behavior under varying concentrations and temperatures.

Unrevealed works: Extensive research on nanofluid is carried out for the combined effect of thermophoresis, mixed convection, radiation, and chemical species in nanofluid over exponentially stretching surface have received limited attention. Existing studies focus on simplified geometries neglecting the thermophoretic particle deposition and the role of motile microorganisms in enhancing heat and mass transfer. Further, very few works have utilized spectral quasilinearization method to handle the governing equations.

Aim of the research: The major goal of the proposed investigation is to carry out the thermophoretic particle deposition in a mixed convective bioconvection flow through an exponentially elongating sheet embedding a permeable matrix accounting for radiation, heat source and chemical reaction. This aims to;

- Developed a mathematical model incorporating the effects of thermophoresis, bioconvection and mixed convection.
- Solve the coupled differential equations using Spectral Quasilinearization Method to exhibits high accuracy and computational accuracy.
- Analyzing the influence of im portant factors like thermophoretic coefficient, radiation, permeability, and chemical reaction on the flow characteristics.

Novelty: The proposed investigation shows its novelty due to the mathematical model and analyzing the incorporation of thermophoretic particle deposition in bioconvective flow over an exponentially stretching sheet embedding within porous matrix. The innovative concept presented here as;

- The integration of thermophoresis and bioconvection effects which are typically studied in better presentation of particle deposition, transport in the fluid flow system.
- The application of SQLM to solve the nonlinear coupled equations in analyzing the problem with greater accuracy.

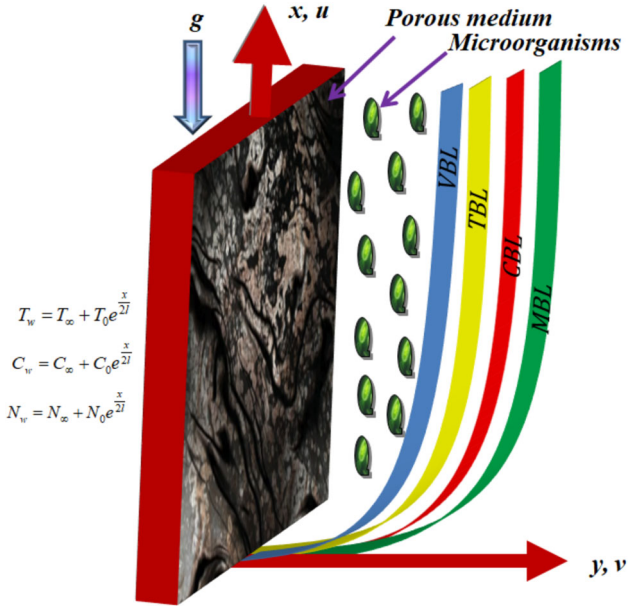

Fig. 1 Flow geometry

- The combined impact of thermal radiation, chemical reaction, and heat source shows a significant enhancement in the flow characteristics.
- Several practical applications from which the proposed topic is useful in the area of biomedical i.e., targeted drug delivery process.

2 Mathematical formulation

The bioconvective nanofluid flow through an exponential two-dimensional stretching surface is proposed in the current study. The flow via a permeable medium encompasses with the impact of thermophoretic particle deposition is affected by the heat source and chemical species. The main flow direction is assumed to be x-axis placed vertically along the direction of the stretching surface and the stretching velocity is considered as $U = U_1 e^{x/l}$. Further, the y direction of the coordinate system is normal to the main flow direction. The surface temperature as well as concentration are varying exponentially and those are presented as $T_w = T_\infty + T_0 e^{x/2l}$ and $C_w = C_\infty + C_0 e^{x/2l}$ respectively where T_0 and C_0 are the reference temperature and concentration. In particular, the ambient state conditions are T_∞ and C_∞ successively. In similar, $N_w = N_\infty + N_0 e^{x/2l}$ is also considered as is a variable wall conditions for the concentration of the motile microorganism with N_0 as the reference concentration and N_∞ is the ambient state conditions (see Fig. 1). For the aforesaid assumptions the governing flow model is presented as (Prasannakumara et al. 2023):

$$u_x + v_y = 0 \tag{1}$$

$$uu_x + vu_y = u_{yy}\upsilon - \frac{\upsilon}{Kp^*}u + g\left\{\begin{array}{l}(T - T_\infty)\left(\gamma_1 + \gamma_2 (T - T_\infty)\right) + \\ (C - C_\infty)\left(\gamma_3 + \gamma_4 (C - C_\infty)\right) + \\ (N - N_\infty)\left(\gamma_5 + \gamma_6 (N - N_\infty)\right)\end{array}\right\} \tag{2}$$

$$uT_x + vT_y = \frac{1}{\rho Cp}\left(\kappa + \frac{16\sigma^* T_\infty^3}{3k^*}\right)T_{yy} + \frac{Q^*}{\rho Cp}(T - T_\infty) \tag{3}$$

$$uC_x + vC_y = D_B C_{yy} - \left(V_T (C - C_\infty)\right)_y - Kr(C - C_\infty) \tag{4}$$

$$uN_x + vN_y + \frac{bW_c}{C_w - C_\infty}\left[\left(NC_y\right)_y\right] = D_m N_{yy} \tag{5}$$

Further, the related surface constraints are:

$$\left.\begin{array}{ll} u = U,\ v = -v(x) = -v_0 e^{\frac{x}{2l}},\ C = C_w,\ T = T_w,\ N = N_w & at\ y = 0 \\ u \to 0,\ C \to C_w,\ N \to N_\infty,\ T \to T_\infty & as\ y \to \infty \end{array}\right\} \tag{6}$$

where the considered porous matrix along with the heat source is considered to be varying exponentially and the expression $Kp^* = Kpe^{-x/l}$ is the permeability, $Q = Q_0 e^{-x/l}$ is proposed heat source/sink. The analyzed thermophoretic velocity V_T is expressed a $V_T = -\frac{k\upsilon_{nf}}{T_r}e^{-x/2l}\frac{\partial T}{\partial y}$ in which T_r indicates reference temperature and the constant k is denoted as thermophoretic coefficient. Particularly, $v_0 e^{-x/2l}$ indicates the mass suction due to the permeable sheet. Kr, swimming speed of the microorganisms is represented as Wc, Brownian diffusion D_B, Solutal Diffusion coefficient D_m respectively.

The transformations containing the similarity function and the stream function used in the above flow phenomena are (Fuzhang et al. 2022);

$$\left.\begin{array}{c} \eta = \sqrt{\frac{U_1}{2\upsilon_f l}}\, y e^{-\frac{x}{2l}},\ \psi = \sqrt{2\upsilon_f U_1 l}\, e^{-\frac{x}{2l}} f(\eta), \\ u = f(\eta) e^{-\frac{x}{l}} U_1,\ v = -\sqrt{\frac{\upsilon_f U_1}{2l}}\, e^{-\frac{x}{2l}}\left(f(\eta) + \eta f(\eta)\right), \\ T = T_\infty + (T_w - T_\infty)\theta(\eta),\ C = C_\infty + (C_w - C_\infty)\chi(\eta), \\ N = N_\infty + (N_w - N_\infty)\phi(\eta) \end{array}\right\} \tag{7}$$

The introduction of above said similarity rule that holds good for the continuity equation and further using in Eqs. (2, 3, 4, 5) with surface condition Eq. (7), the transformed

non-dimensional fomr of the model are;

$$f''' - Daf' + \begin{vmatrix} f & 2f' \\ f' & f'' \end{vmatrix} + \lambda((1+\lambda_1\theta)\theta + Gr(1+\lambda_2\chi)\chi + Gc(1+\lambda_3\phi)\phi) = 0 \tag{8}$$

$$(1+Nr)\theta'' + \Pr\begin{vmatrix} f & \theta \\ f' & \theta' \end{vmatrix} + 2\Pr Q\theta = 0 \tag{9}$$

$$\chi'' + Le\Pr\begin{vmatrix} f & \chi \\ f' & \chi' \end{vmatrix} - \tau Le\Pr\begin{vmatrix} \chi & -\theta' \\ \chi' & \theta'' \end{vmatrix} - Le\Pr Kc\chi = 0 \tag{10}$$

$$\phi'' + Lb\Pr\begin{vmatrix} f & \phi \\ f' & \phi' \end{vmatrix} - Pe\begin{vmatrix} \chi' & -\chi'' \\ \sigma_1+\phi & \phi' \end{vmatrix} = 0 \tag{11}$$

Moreover, the surface conditions are reduced to;

$$\left.\begin{array}{l} f'(0)=1,\ \theta(0)=1,\ \chi(0)=1,\ f(0)=S,\ \phi(0)=1,\ \eta=0, \\ f'(\infty)=0,\ \theta(\infty)=0,\ \chi(\infty)=0,\ \phi(\infty)=0 \qquad ,\ \eta\to\infty \end{array}\right\} \tag{12}$$

The transformed model equipped with the non-dimensional factors are described as;

$$\left.\begin{array}{l} Da=\dfrac{2\upsilon_f l}{K_0U_1},\ Q=\dfrac{Q_0 l}{U_1},\ \tau=-\dfrac{K}{T_r}(T_w-T_\infty), \\ Lb=\dfrac{\alpha}{D_m},\ S=\upsilon_0\sqrt{\dfrac{2l}{U_1\upsilon_f}},\ Kc=l\dfrac{Kr}{U_1} \\ Pe=\dfrac{bW_c}{U_1},\ \sigma_1=\sigma^* e^{x/2l}\left(\sigma^*=\dfrac{N_\infty}{N_w-N_\infty}\right), \\ Le=\dfrac{\alpha_f}{D_B},\ \Pr=\dfrac{\mu Cp}{\kappa},\ \lambda=\dfrac{Gr_T}{\mathrm{Re}_x^2},\ \lambda_1=\dfrac{\gamma_2(T_w-T_\infty)}{\gamma_1}, \\ \lambda_2=\dfrac{\gamma_4(C_w-C_\infty)}{\gamma_3},\ \lambda_3=\dfrac{\gamma_6(N_w-N_\infty)}{\gamma_5},\ Gr=\dfrac{Gr_C}{Gr_T}, \\ Gr_C=\dfrac{g^*\gamma_3(C_w-C_\infty)}{\upsilon^2},\ Gc=\dfrac{Gr_N}{Gr_T},\ Gr_N=\dfrac{g^*\gamma_5(N_w-N_\infty)}{\upsilon^2} \\ Nr=\dfrac{16\sigma^*T_\infty^3}{k^*\kappa} \end{array}\right\} \tag{13}$$

Engineering coefficients:

$$Cf_x=\frac{2\tau_w U_1^{-2}}{\rho_f},\ Nu_x=\frac{lq_w}{(T_w-T_\infty)}, \quad Sh_x=\frac{lq_m}{D_B(C_w-C_\infty)},\ Nn_x=\frac{lq_n}{(N_w-N_\infty)} \tag{14}$$

The terms τ_x, q_w, q_m and q_n

$$\tau_x=\left(\frac{\partial u}{\partial y}\right)_{y=0}\mu_{nf},\ q_w=-k_{nf}\left(\frac{\partial T}{\partial y}\right)_{y=0}+(q_r)_{y=0}, \quad q_m=-\left(\frac{\partial C}{\partial y}\right)_{y=0}D_f,\ q_n=-\left(\frac{\partial N}{\partial y}\right)_{y=0}D_m, \tag{15}$$

The reduced equations are

$$\mathrm{Re}^{0.5}Cf_x=f''(0),\ \mathrm{Re}^{-0.5}Nu_x=-(1+Nr)\theta'(0), \quad \mathrm{Re}^{-0.5}Sh_x=-\chi'(0),\ \mathrm{Re}^{-0.5}Nn_x=-\phi'(0) \tag{16}$$

where $\mathrm{Re}=\frac{U_1 e^{\frac{x}{l}} l}{2\upsilon_f}$ is local Reynolds number.

3 Proposed methodology

The proposed modeled Eqs. (8, 9, 10, 11) are nonlinear and coupled those are exposed to the equivalent surface conditions Eq. (12) are handled numerically by utilizing the "*Spectral Quasi-linearization Method*" (SQLM) and the outcomes are attained by using the codes in MATLAB. In the proposed methodology it includes the linearization of the non-linear ODEs and then the "*Newton–Raphson-based Quasi-linearization Method*" (QLM) which was first introduced by Bellman and Kalaba (1965) in 1965. Further, Taylor series is utilised in the process of linearization with the assumption of a close difference within the considered the unknown function presented at the iteration level $(p+1)$ and then the value at the earlier iteration level (p), (see Motsa 2013 (Wang et al. 2024)). Further, the discretized system of equations is handled by utilizing the "*Chebyshev spectral collocation*" method for enhanced computational efficiency and accuracy. This process is conducted iteratively to ensure rapid convergence and provide accurate solutions. Applying the QLM on (8, 9, 10, 11) results in a new system of equations:

$$a_{0,p}f'''_{p+1}+a_{1,p}f''_{p+1}+a_{2,p}f'_{p+1}+a_{3,p}f_{p+1}+a_{4,p}\theta_{p+1}+a_{5,p}\chi_{p+1}=V_1 \tag{17}$$

$$b_{0,p}\theta''_{p+1}+b_{1,p}\theta'_{p+1}+b_{2,p}\theta_{p+1}+b_{3,p}f'_{p+1}+b_{4,p}f_{p+1}=V_2 \tag{18}$$

$$c_{0,p}\chi''_{p+1}+c_{1,p}\chi'_{p+1}+c_{2,p}\chi_{p+1}+c_{3,p}f'_{p+1}+c_{4,p}f_{p+1}+c_{5,p}\theta''_{p+1}+c_{6,p}\theta'_{p+1}=V_3 \tag{19}$$

$$d_{0,p}\phi''_{p+1}+d_{1,p}\phi'_{p+1}+d_{2,p}\phi_{p+1}+d_{3,p}f'_{p+1}+d_{4,p}f_{p+1}+d_{5,p}\chi''_{p+1}+d_{6,p}\chi'_{p+1}=V_4 \tag{20}$$

The variable coefficients $a_{r,p}$, $b_{r,p}$, $c_{r,p}$ and $d_{r,p}$ ($where\ r = 1, 2, 3, ..$) are known, which are given by:

$$\left.\begin{aligned}
&a_{0,p} = 1,\ a_{1,p} = f_p a_{2,p} = -4f'_p - Da,\\
&\quad a_{3,p} = f''_p,\ a_{4,p} = \lambda(1 + 2\lambda_1\theta_p),\\
&a_{5,p} = \lambda Gr(1 + 2\lambda_2\chi_p),\ b_{0,p} = 1 + Nr,\\
&\quad b_{1,p} = \Pr f_p b_{2,p} = -\Pr f'_p,\\
&\quad b_{3,p} = -\Pr\theta_p,\ b_{4,p} = \Pr\theta'_p,\\
&c_{0,p} = 1,\ c_{1,p} = Le\Pr f'_p - \tau Le\Pr\theta'_p,\\
&\quad c_{2,p} = -Le\Pr f'_p - \tau Le\Pr\theta'_p - Le\Pr Kc,\\
&\quad c_{3,p} = -Le\Pr\chi_p,\\
&c_{4,p} = Le\Pr\chi'_p,\ c_{5,p} = -\tau Le\Pr\chi_p,\\
&\quad c_{6,p} = -\tau Le\Pr\chi'_p,\\
&\quad d_{0,p} = 1,\ d_{1,p} = \Pr Lbf_p - Pe\chi'_p,\\
&d_{2,p} = -\Pr Lbf'_p - Pe\chi''_p,\ d_{3,p} = -\Pr Lb\phi_p,\\
&\quad d_{4,p} = \Pr Lb\phi'_p,\ d_{5,p} = -Pe(\sigma_1 + \phi_p),\\
&\quad d_{6,p} = -Pe\phi'_p.
\end{aligned}\right\} \tag{21}$$

The right-hand side of Eqs. (26–30) are given as:

$$V_1 = a_{0,p}f'''_p + a_{1,p}f''_p + a_{2,p}f'_p + a_{3,p}f_p + a_{4,p}\theta_p + a_{5,p}\phi_p - R_f$$

$$V_2 = b_{0,p}\theta''_p + b_{1,p}\theta'_p + b_{2,p}\theta_p + b_{3,p}f'_p + b_{4,p}f_p - R_\theta$$

$$V_3 = c_{0,p}\chi''_p + c_{1,p}\chi'_p + c_{2,p}\chi_p + c_{3,p}f'_p + c_{4,p}f_p + c_{5,p}\theta''_p + c_{6,p}\theta'_p - R_\chi$$

$$V_4 = d_{0,p}\phi''_p + d_{1,p}\phi'_p + d_{2,p}\phi_p + d_{3,p}f'_p + d_{4,p}f_p + d_{5,p}\chi''_p + d_{6,p}\chi'_p - R_\phi$$

where

$$R_f = f'''_p + f_p f'_p - 2f^2_p + \lambda((1 + \lambda_1\theta_p)\theta_p + Gr(1 + \lambda_2\chi_p)\chi_p + (1 + \lambda_2\phi_p)\phi_p - Daf'_p,$$

$$R_\theta = (1 + Nr)\theta''_p + Pr\left(f_p\theta'_p - f'_p\theta_p\right) + 2PrQ\theta_p$$

$$R_\chi = \chi''_p + LePr\left(f_p\chi'_p - f'_p\chi_p\right) - \tau LePr\left(\chi_p\theta''_p + \theta'_p\chi'_p\right) - LePrKc\chi_p,$$

$$R_\phi = \phi''_p + LbPr\left(f_p\phi'_p - f'_p\phi_p\right) - Pe\left(\chi'_p\phi'_p + \chi''_p(\sigma_1 + \phi_p)\right). \tag{22}$$

By employing suitable initial guesses, the iteration schemes (17)—(20) are iteratively solved to obtain f_{p+1}, θ_{p+1}, χ_{p+1} and ϕ_{p+1}. The appropriate initial guesses in this case are given as:

$$f_0(\eta) = 1 + S - e^{-\eta},\ \theta_0(\eta) = e^{-\eta},\ \chi_0(\eta) = e^{-\eta},\ \phi_0(\eta) = e^{-\eta}. \tag{23}$$

To numerically solve Eqs. (17) - (20), the Chebyshev spectral collocation method is utilized for discretization. This approach operates within the interval [-1, 1], where computations are performed. Since the original domain of the problem is semi-infinite, a domain truncation is required before implementing the spectral method. The semi-infinite domain is approximated by a finite domain [0, L], where L is chosen large enough to capture the characteristics of the solution at infinity. To facilitate this, the transformation $\eta = \frac{L(\xi+1)}{2}$ is introduced, which maps the truncated domain [0, L] onto the interval [-1, 1]. This mapping allows for the employing the proposed method on a finite domain while maintaining the accuracy of the solution.

Furthermore, a derivative matrix $\boldsymbol{D}$ is implemented to estimated derivatives of the unidentified functions $f(\eta)$, $\theta(\eta)$, $\chi(\eta)$ and $\phi(\eta)$ at the specified collocation points. This approximation is performed by computing a matrix–vector product, described as:

$$\left.\begin{aligned}
&\frac{df}{d\eta} = \sum_{p=0}^{N_x} D_{pq} f(\xi_q) = DF,\\
&q = 0, 1, 2, ...N_x,\ \frac{d\theta}{d\eta} = \sum_{p=0}^{N_x} D_{pq}\theta(\xi_q) = D\Theta,\\
&q = 0, 1, 2, ...N_x\\
&\frac{d\chi}{d\eta} = \sum_{p=0}^{N_x} D_{pq}\chi(\xi_q) = DF,\\
&q = 0, 1, 2, ...N_x,\ \frac{d\phi}{d\eta} = \sum_{p=0}^{N_x} D_{pq}\phi(\xi_q) = D\Phi,\\
&q = 0, 1, 2, ...N_x
\end{aligned}\right\} \tag{24}$$

Here, N_x is the total collocation points, $D = 2D/L$, and

$$F = [f(\xi_0),\ f(\xi_1),\ ....,\ f(\xi_{N_x})]^T,$$
$$\Theta = [\theta(\xi_0),\ \theta(\xi_1),\ ....,\ \theta(\xi_{N_x})]^T,$$
$$\chi = [\chi(\xi_0),\ \chi(\xi_1),\ ....,\ \chi(\xi_{N_x})]^T,$$
$$\Phi = [\phi(\xi_0),\ \phi(\xi_1),\ ....,\ \phi(\xi_{N_x})]^T,$$

In matrix notation, the SQLM approach for Eqs. (17, 18, 19, 20) can be succinctly expressed as:

$$\begin{bmatrix} A_{11} & A_{12} & A_{13} & A_{14} \\ A_{21} & A_{22} & A_{23} & A_{24} \\ A_{31} & A_{32} & A_{33} & A_{34} \\ A_{41} & A_{42} & A_{43} & A_{44} \end{bmatrix} \begin{bmatrix} f_{p+1} \\ \theta_{p+1} \\ \chi_{p+1} \\ \phi_{p+1} \end{bmatrix} = \begin{bmatrix} V_1 \\ V_2 \\ V_3 \\ V_4 \end{bmatrix}, \tag{25}$$

Here

$$\left.\begin{aligned} &A_{11} = diag[a_{0,p}]D^3 \\ &\quad +diag[a_{1,p}]D^2 + diag[a_{2,p}]D + diag[a_{3,p}]I, \\ &A_{12} = diag[a_{4,p}]I \\ &A_{13} = 0,\ A_{14} = diag[a_{5,p}]I,\ A_{12} = diag[b_{3,p}]D \\ &\quad +diag[b_{4,p}]I, \\ &A_{22} = diag[b_{0,p}]D^2 + diag[b_{1,p}]D^2 \\ &\quad +diag[b_{2,p}]I,\ A_{23} = 0,\ A_{24} = 0, \\ &A_{31} = diag[c_{3,p}]D^2 + diag[c_{4,p}]I, \\ &A_{32} = diag[c_{5,p}]D^2 \\ &\quad +diag[c_{6,p}]D^2,\ A_{33} = diag[c_{0,p}]D^2 \\ &\quad +diag[c_{1,p}]D + diag[c_{2,p}]I,\ A_{34} = 0. \\ &A_{41} = diag[d_{3,p}]D + diag[d_{4,p}]I, \\ &A_{42} = 0,\ A_{43} = diag[d_{5,p}]D^2 + diag[d_{6,p}]D, \\ &A_{44} = diag[d_{0,p}]D^2 + diag[d_{1,p}]D \\ &\quad +diag[d_{2,p}]I. \end{aligned}\right\}$$

In the above representation, the symbol $diag$ indicates a diagonal matrix with dimensions $(N_x + 1) \times (N_x + 1)$ I denotes an identity matrix of size $(N_x + 1) \times (N_x + 1)$, O represents $(N_x + 1) \times (N_x + 1)$ zero matrix and D signifies derivative with respect to η.

4 Results and discussion

In this section, we analyse the numerically simulated outcomes obtained using spectral quasi-linearization method through codes written and executed in MATLAB for the problem of 2D laminar flow of an incompressible nanoliquid over an elastic stretching sheet (ESS) filled with porous. The numerical approach efficiently solves the standard equations for different flow profiles. The results of this study were cross-referenced with data from earlier published works as seen in Table 1 to ensure the accuracy and validity of our findings, which are in admirable agreement with those disclosed in referenced works. To demonstrate the convergence of the "*Spectral Quasi-linearization Method*" (SQLM), we analyzed the solution errors in terms of the infinity norms,

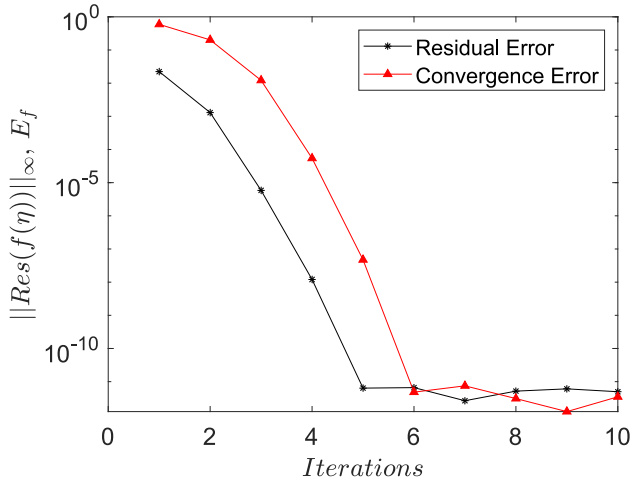

Fig. 2 Solution and residual errors for $f(\eta)$

which indicate the differences in function values between consecutive iterations described as follows:

$$E_f = \max_{0\le j\le N_x} \|f_{p+1,j} - f_{p,j}\|_\infty,\ E_\theta = \max_{0\le j\le N_x} \|\theta_{p+1,j} - \theta_{p,j}\|_\infty,$$
$$E_\chi = \max_{0\le j\le N_x} \|\chi_{p+1,j} - \chi_{p,j}\|_\infty,\ E_\phi = \max_{0\le j\le N_x} \|\phi_{m+1,r} - \phi_{m,j}\|_\infty.$$

To further authenticate the correctness of the SQLM, the infinity norm of the residual error for each function is evaluated. This process involves inserting the estimated results into the governing differential Eqs. (8) through (11). The corresponding norms are defined as follows:

$$\begin{aligned} \|\mathrm{Res}\,(f)\ \|_\infty = \|&f_p''' + f_p f_p'' - 2f_p^2 \\ &+ \lambda\left(1+\lambda_1\theta_p\right)\theta_p + Gr\left(1+\lambda_2\phi_p\right)\phi_p \\ &+ (1+\lambda_2 H)\,H - Daf_p'\|_\infty, \end{aligned}$$

$$\begin{aligned} \|\mathrm{Res}\,(\theta)\ \|_\infty = \|&(1+Nr)\,\theta_p'' + \mathrm{Pr}\left(f_p\theta_p' - f_p'\theta_p\right) \\ &+ 2\,\mathrm{Pr}\,Q\theta_p\|_\infty, \end{aligned}$$

$$\begin{aligned} \|\mathrm{Res}\,(\chi)\ \|_\infty = \|&\chi_p'' + Le\,\mathrm{Pr}\left(f_p\chi_p' - f_p'\chi_p\right) \\ &- \tau Le\,\mathrm{Pr}\left(\chi_p\theta_p'' + \theta_p'\chi_p'\right) \\ &- Le\,\mathrm{Pr}\,Kc\chi_p\|_\infty \end{aligned}$$

$$\begin{aligned} \|\mathrm{Res}\,(\phi)\ \|_\infty = \|&\phi_p'' + Lb\,\mathrm{Pr}\left(f_p\phi_p' - f_p'\phi_p\right) \\ &- Pe\left(\chi_p'\phi_p' + \chi_p''\left(\sigma_1+\phi_p\right)\right)\|_\infty, \end{aligned}$$

Figures 2, 3, 4, 5 provide a comprehensive visualization of decreases in both convergence and residual errors as the iterations increases, clearly demonstrating the remarkable accuracy and efficiency of the "Spectral Quasi-linearization Method (SQLM)". These figures illustrate the rapid decline in errors, highlighting how SQLM quickly approaches a

Table 1 Comparison of $-\theta'(0)$, with previously published work of Ref. (Magyari and Keller 1999), Ref. (Bidin and Nazar 2009), Ref. (Prasannakumara et al. 2023), Ref. (Ishak 2011), Ref. (Mukhopadhyay and Gorla 2012), and Ref. (Abd El-Aziz 2009), for different values of Pr

Pr	Ref. (Magyari and Keller 1999)	Ref. (Bidin and Nazar 2009)	Ref. (Prasannakumara et al. 2023)	Ref. (Ishak 2011)	Ref. (Mukhopadhyay and Gorla 2012)	Ref. (Abd El-Aziz 2009)	Present study
1.0	0.954782	0.9547	0.954955	0.9548	0.9547	0.954785	0.95478543
2.0		1.4714	1.471420	1.4715	1.4714		1.47142031
3.0	1.869075	1.8691	1.8690441	1.8691	1.8691	1.869074	1.869074352
5.0	2.500135		2.500108	2.5001	2.5001	2.500132	2.50013217
10.0	3.660379		3.6603543	3.6604	3.6604	3.660372	3.66037215

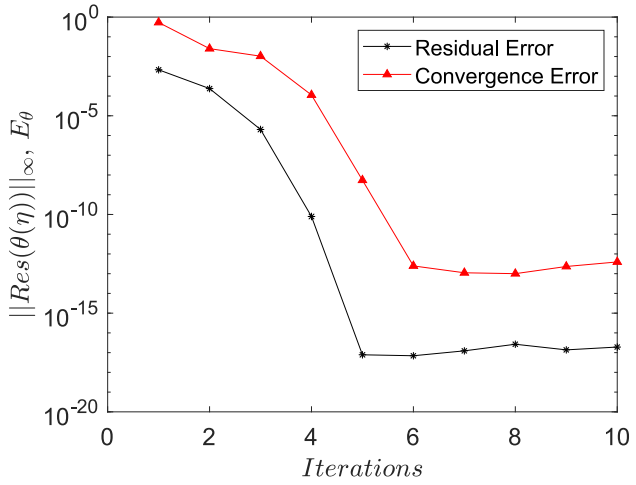

Fig. 3 Solution and residual errors for $\theta(\eta)$

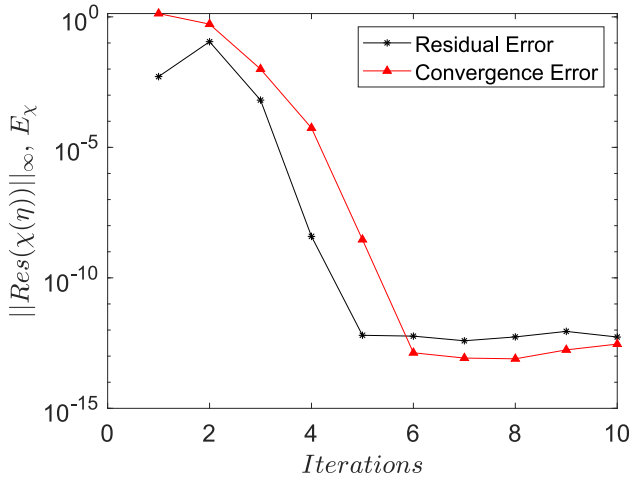

Fig. 4 Solution and residual errors for $\chi(\eta)$

highly accurate solution within a minimal number of iterations. Specifically, the residual and convergence errors achieve very low values, after about 6 to 7 iterations. This behaviour suggests that the SQLM delivers not only highly accurate but also swiftly converging solutions, making it a

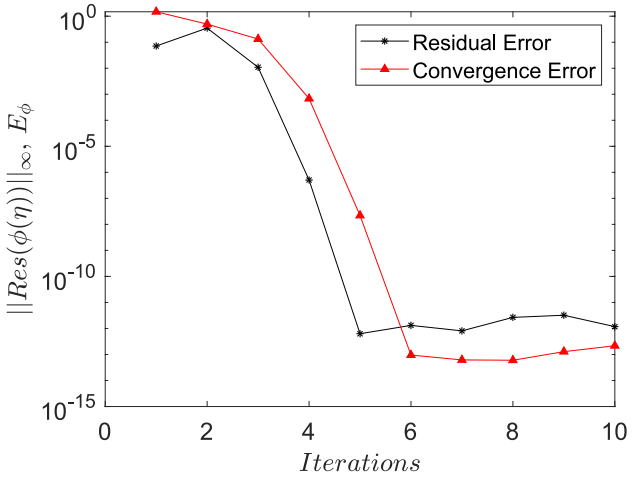

Fig. 5 Solution and residual errors for $\phi(\eta)$

powerful numerical tool for the solution. The fast rate of error reduction indicates that the method efficiently refines the approximate solutions with each iteration, achieving precision without requiring excessive computational time.

Furthermore, the figures underscore the effectiveness of SQLM in terms of both error minimization and overall stability. The residual error, representing the transformation between the numerical solution and the exact solution, falls rapidly, signifying that the method accurately approximates the true solution. Simultaneously, the convergence error, which measures the differences between successive iterations, also approaches zero after a small number of iterations, confirming that the numerical solution has stabilized, and further iterations yield negligible changes.

The parametric variation of several factors on the flow phenomena are presented in Figs. 6, 7, 8, 9, 10, 11, 12, 13, 14, 15, 16, 17, 18, 19, 20, 21, 22, 23 including the shear drag rate, heat and solutal transfer rate respectively. Figure 6 exhibits the crucial properties of the Darcy parameter on the fluid flow via porous medium which characterizes the relative importance of the penetrability on the velocity profile. To portray the characteristic of Darcy number, Da the parametric range

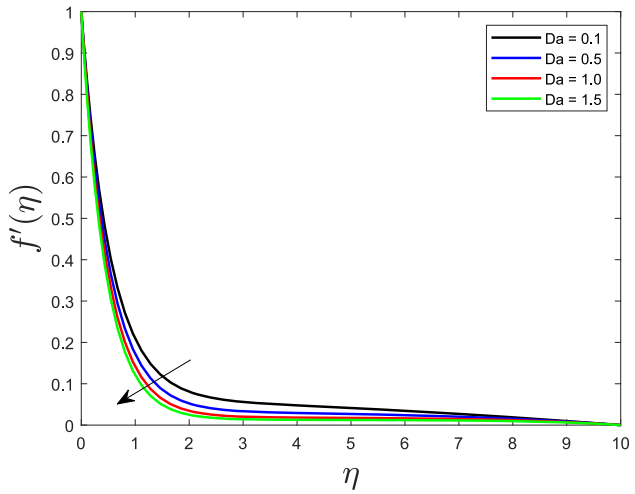

Fig. 6 Influence of Da on velocity distribution

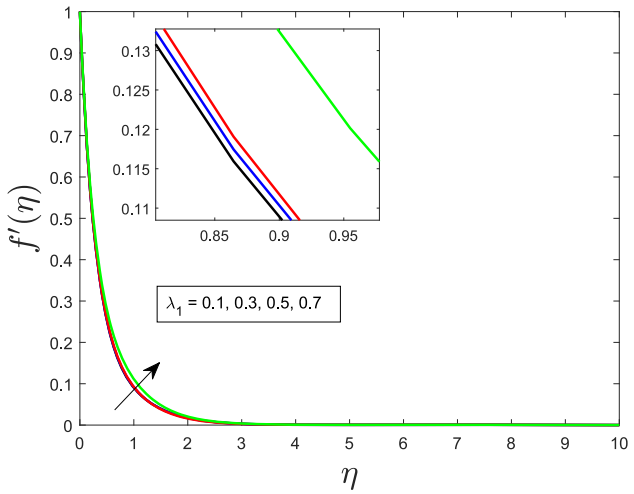

Fig. 9 Characteristic of λ_1 on fluid velocity

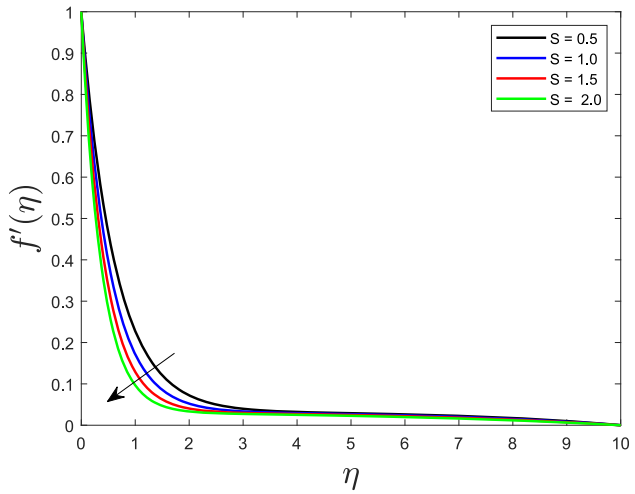

Fig. 7 Influence of S on velocity distribution

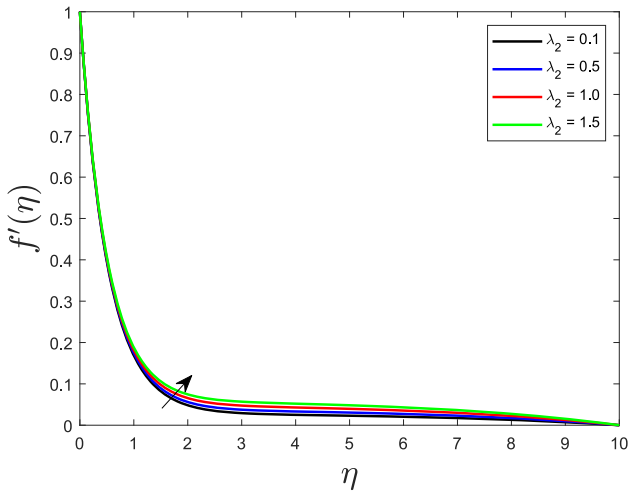

Fig. 10 Role of λ_2 on fluid velocity

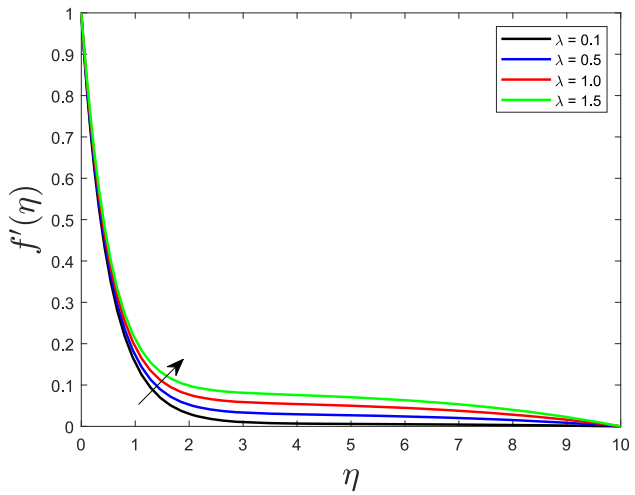

Fig. 8 Behavior of λ on velocity

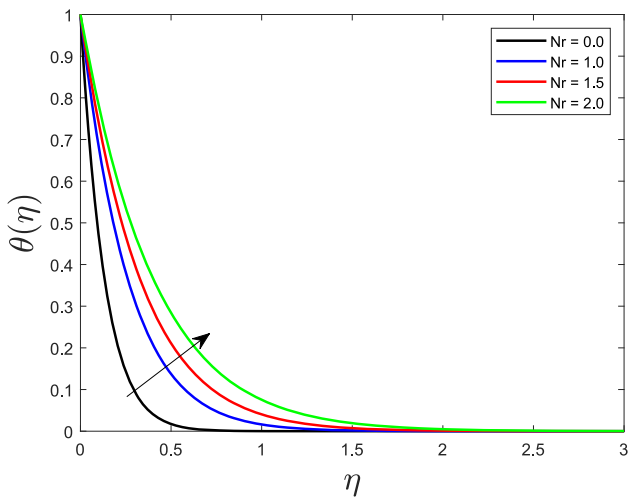

Fig. 11 Influence of Nr on thermal distribution

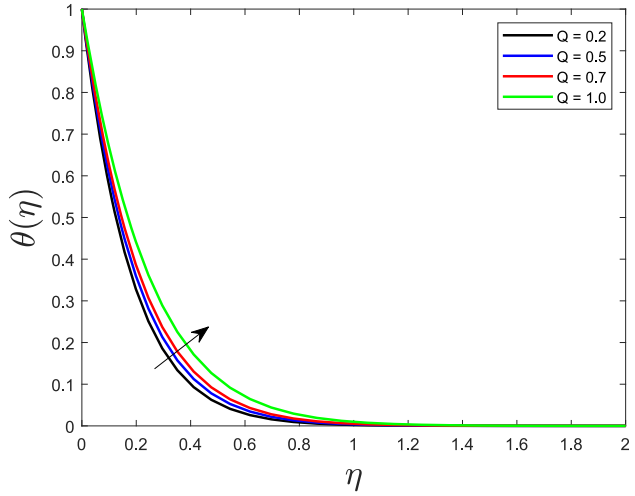

Fig. 12 Influence of Q on thermal distribution

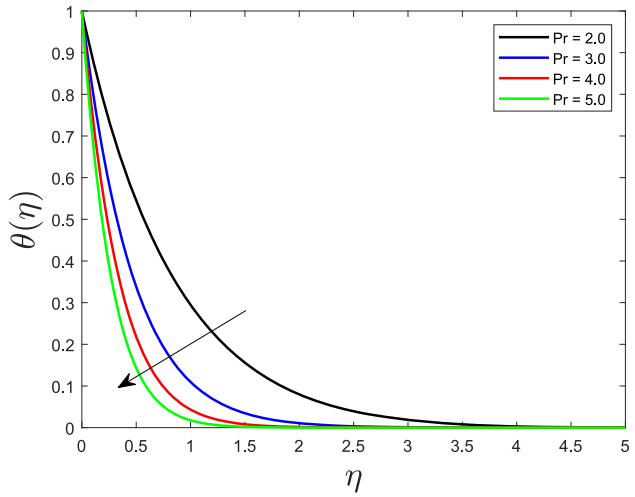

Fig. 13 Influence of Pr on thermal distribution

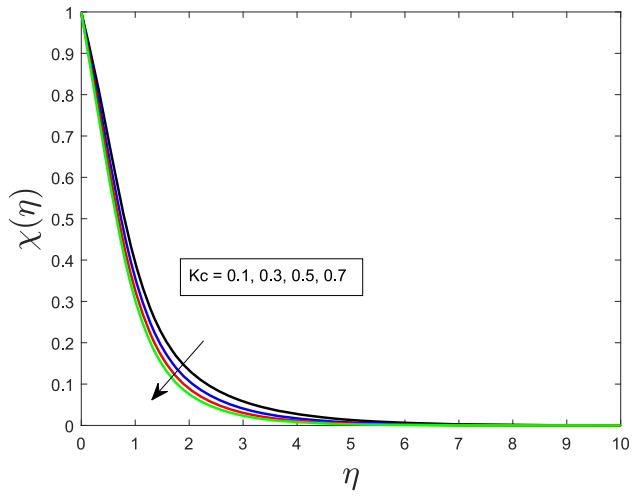

Fig. 14 Influence of Kc on concentration distribution

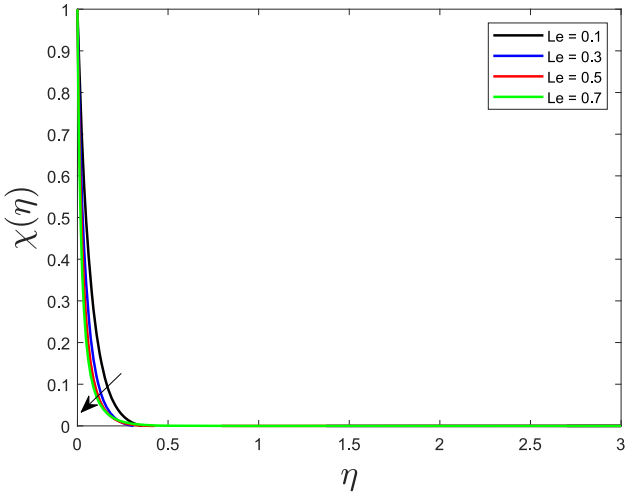

Fig. 15 Influence of Le on concentration distribution

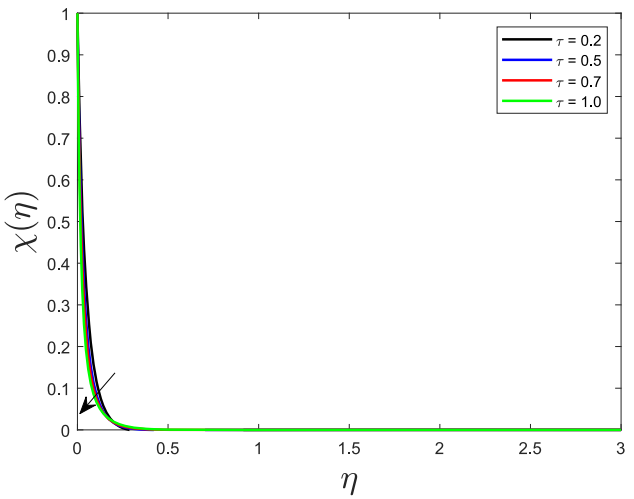

Fig. 16 Influence of τ on concentration distribution

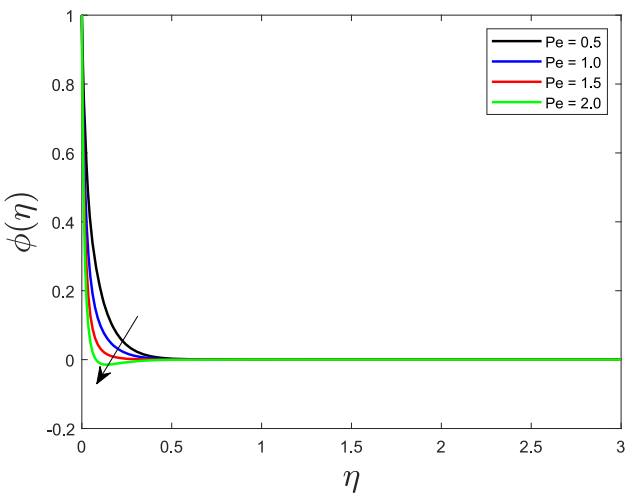

Fig. 17 Influence of Pe on motile microorganism distribution

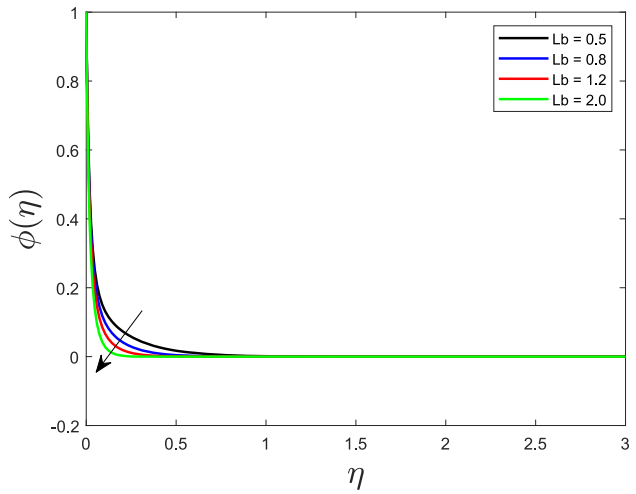

Fig. 18 Influence of Lb on motile microorganism distribution

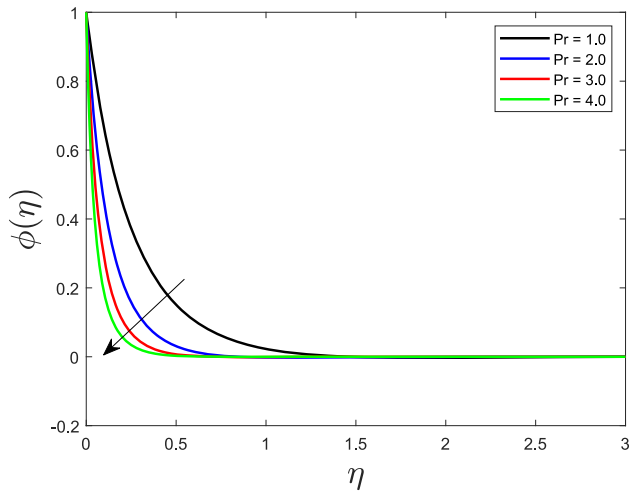

Fig. 19 Influence of Pr on motile microorganism distribution

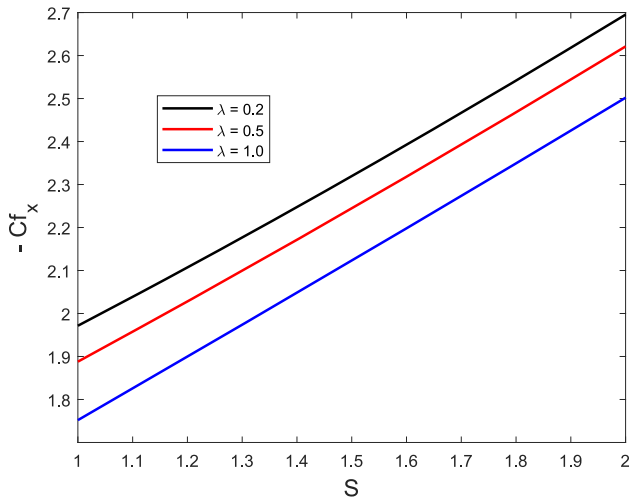

Fig. 20 Variation in $-Cf_x$ with λ_2 and S

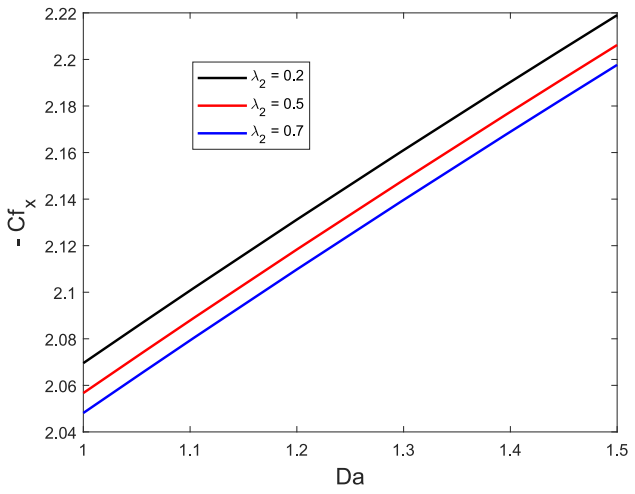

Fig. 21 Variation in $-Cf_x$ with λ_2 and Da

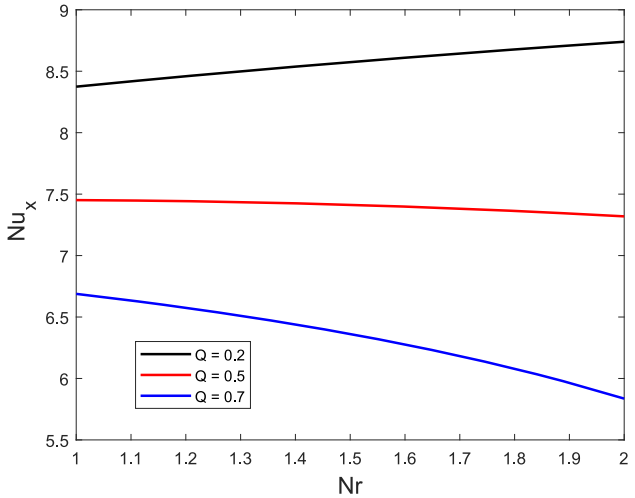

Fig. 22 Variation in Nu_x with Q and Nr

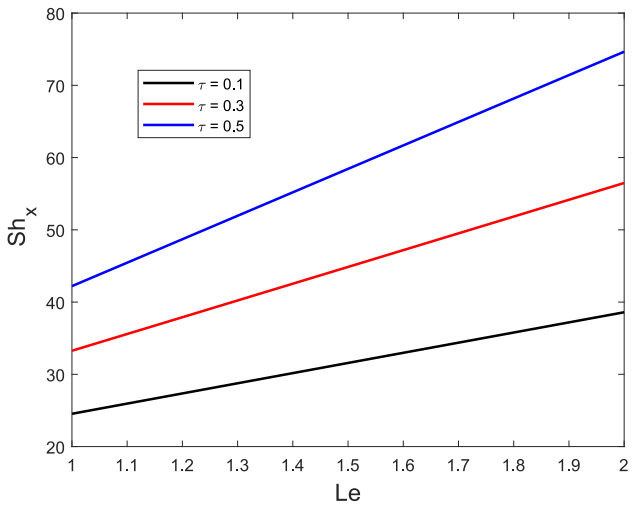

Fig. 23 Variation in Sh_x with Le and τ

is considered as $0.1 \leq Da \leq 1.5$. The low Darcy number ($Da = 0.1$) indicates a porous medium with low permeability which means the medium offers insignificant resistance to the fluid flow. This causes the maximum strength of the velocity in magnitude. However, with increasing permeability, the resistance increases which lead to the drag enhances. Therefore, the fluid velocity reduces significantly causing a significant retardation in the bounding surface thickness. A higher Darcy number shows a thinner in the thickness of the profile and as the domain heightened the profile becomes smooth and ceases to meet the appropriate boundary condition.

The noteworthy impact of the suction parameter affecting fluid velocity of the Casson fluid is presented in Fig. 7. The contribution of factor S is deployed within the numerical range as $0.5 \leq S \leq 2$. The visualization of the figure shows that, as growth in the suction parameter a significant deceleration in the fluid flow is rendered. The inclusion of suction effectively removes fluid from the bounding surface causing a retardation in the surface thickness and also reducing the momentum of the fluid near the surface. Further, higher suction is useful in preventing the formation of flow stabilization near to the surface. This reduction is due to fluid drawing towards the surface for the increasing suction that suppresses the free-stream velocity. In other words, the presence of suction enhances the wall shear stress since it suppresses the velocity close to the surface.

The mixed convection consequence occurs because of the influential characteristic of the buoyant forces on the fluid momentum. The inclusion of thermal, solutal well as motile microorganisms shows the effect of buoyancy on the flow profiles. Figures 8, 9, 10 exhibit the structural properties of the buoyancy ratio, thermal buoyancy, and mixed convection parameters affecting the fluid velocity respectively. The buoyancy ratio, λ presented as $0.1 \leq \lambda \leq 1.5$, the thermal buoyancy,$\lambda_1$ portrays within the range $0.1 \leq \lambda_1 \leq 0.7$ and finally, the mixed convection behaviour is depicted within the range of $0.1 \leq \lambda_2 \leq 1.5$ respectively to exhibit their impact on the velocity profile. The density variations between the layers lead to show the impact of buoyancy on the profile. This difference in density leads to a pressure differential where the bottom layer pressure dominates the pressure at the upper layer which gives rise to exhibits the role of buoyancy. The buoyancy ratio shows the relationship between the thermal and solutal buoyancy, which favors increasing thermal buoyancy for the increasing ratio. The positive sign indicates both occur along the same direction resulting in enhanced velocity leading to an upward trend with a peak velocity closer to the surface. Further, thermal buoyancy is driven by the temperature differences in natural convection problems. With the increasing thermal buoyancy, due to greater temperature difference, the upward force becomes stronger which drives faster flow close to the surface with higher peak velocity. The mixed convection restriction defines the ratio of buoyancy forces to the inertia forces. The low convection parameter, the forced convection dominates over buoyancy effects which diminishes the velocity distribution and the thickness of the surface decreases. However, increasing mixed convection, the buoyancy forces start dominating the force convection which provides a larger augmentation in the velocity field throughout the domain.

The heat transfer properties are also affected by the interaction of several influences likely radiation, heat source, and Prandtl number. The behaviour of the radiative heat for the impact of thermal radiation on the thermal field is exhibited in Fig. 11**.** The characteristic is presented by deploying the numerical range of the factor as $0 \leq Nr \leq 2$. Here, the numerical result $Nr = 0$ signifies the absence of thermal radiation and the non-zero values presents the behaviour as a comparative analysis on the fluid temperature. The analysis is presented for the assumption of the heat flux by Rosseland approximation and the nonlinear variation of the temperature is linearized by the Taylor series approximation. The dimensionless favour significantly enhances the thermal field for the increasing radiation. It is the measure of the emitted electromagnetic wave from the fluid element. This emitted electromagnetic wave transformed into heat energy generally termed as thermal radiation which causes a significant transformation of the energy from the surface region. This causes the cooling of the surface as well as the increasing temperature at all points within the domain. Figure 12 exhibits the contribution of the external heat source employed in the energy profile which has significant impact on the thermal distribution. The range of the factor, heat source Q is deployed as $0.2 \leq Q \leq 2$. The positive sign indicates the impact of heat source that affect the profile and this is due to the dominance of the fluid temperature over the free stream temperature. Therefore, increasing heat source led to transfer of the heat from the lower region to the upper i.e., toward the ambient state. The stored energy near the surface moves away from the surface causing a cooling in the surface vis-à-vis the hike in the fluid temperature. This fact is useful in several industrial production process to get a quality product without damaging more products. In both the scenario of heat source and thermal; radiation the enhanced fluid temperature provides a greater increase in the thermal bounding surface thickness also.

The role of thermal conductivity which helps in transforming the heat energy led to exhibit the consequence of Prandtl number on the fluid temperature. Figure 13 demonstrates the characteristic of the Prandtl number on the profile of thermal energy. To exhibit the impact, the Pr values are restricted within the range of $Pr \in [2, 5]$. The non-dimensional quantity Pr is expressed as the ratio of the kinematic viscosity with the thermal diffusivity. The increasing numerical values in Pr suggest the deceleration of the thermal diffusivity

or in other words the enhancement of the kinematic viscosity. Therefore, the reduction in the thermal diffusivity leads to a reduction in the fluid temperature causing a significant deceleration in the thermal bounding surface thickness.

The solutal profile of the Casson fluid is couple with both the flow heat transfer profiles is also affected by the factors involved in it. However, Figs. 14 and 15 show the imposition of the chemical species along with the Lewis number affecting the concentration field. To exhibit the characteristic of the chemical reaction, Kc, the factor varies within the considered range of $0.1 \leq Kc \leq 0.7$ and the range of the Lewis number also varies within the range of $0.1 \leq Le \leq 0.7$. The interaction of additional gases forms the role of chemical species on the profile of concentration. The corroboration of the mathematical expression and the assigned positive values of the reacting agents shows the impact of destructive chemical reactions on the profile. The enhanced chemical reaction leads to have a controlling parametric effect on the concentration distribution. The increase in Kc provides a significant injection of the gaseous element into the fluid which causes a significant retardation in the profile as well as concentration thickness. Further, the factor Lewis number, Le is demonstrated as the relationship between the thermal diffusivity and the solutal diffusivity. The lower in the Lewis number give rise to dominance of the solutal diffusivity over the thermal diffusion which lead to maximum strength in the concentration. Further, the enhancement in Lewis number shows a greater retardation in the solutal diffusion which lead to deceleration the concentration profile within the entire domain.

The impact of the thermophoresis due to the thermophoretic diffusion is presented in Fig. 16 on the concentration distribution. The analysis is deployed for the role of the thermal gradient which affects the fluid concentration distribution. The variation of the thermophoresis on the fluid concentration distribution is presented for the consideration of the numerical range as $0.2 \leq \tau \leq 1$. The increasing the numerical values of the factor also enhances the temperature gradient which lead to supress the fluid temperature distribution throughout.

The impact of solutal Peclet number along with bioconvection Lewis number is depicted in Fig. 17 and Fig. 18 respectively. The factor solutal Peclet number is the ratio of advective transport to the diffusive transport which plays its import role on the motile microorganism distribution. The low Peclet number suggests the diffusion dominates over advection which resulted in the solute spread more uniformly throughout the fluid. This lead to greater concentration away from the motile organism presents in the surface. Further, advection dominates over the diffusion with higher consideration of the Peclet number. This results in the solute being carried primarily by the flow causing more concentration. Therefore, the microorganism profile becomes slower down the profile. Further, the bioconvective Lewis number affects the motile microorganism distribution which is presented in Fig. 19. Physically, Lb is described as the ratio of the thermal diffusivity and the diffusivity of the microorganism particles. The lower Lb presents the dominance of the microorganism diffusivity over the thermal diffusivity for which the profile demonstrates its greater impact in developing the profile whereas for the increasing Lewis number the thermal diffusivity increases as well as the diffusivity of the microorganism retards significantly. This causes a significant attenuation in the profile of the microorganism convection and the profile retards with a greater retardation in the thickness.

5 Conclusions

The flow phenomena for the bioconvection of mixed convective transportation across an exponential stretching surface for the contribution of chemical reaction, thermal radiation, and heat source is analysed in the present study. As a novel approach the thermophoretic particle deposition within the system is also checked thoroughly. The transformed phenomena obtained for the suitable assumption of similarity rules are handled numerically utilizing SQLM and the characteristic of several factors are analysed graphically. The important observations are depicted as below;

- The residual errors obtained for each of the profiles and the comparative study with the earlier investigations lead to show the good association as well as the convergence of the proposed methodology.
- The permeability of the porous matrix and the permeability of the medium favors in a significant attenuation in the fluid momentum of the bioconvective flow.
- The upward thrust due to the inclusion of mixed convection effect gives rise to boost the fluid velocity within the entire region.
- The radiating heat vis-à-vis the imposition of additional heat source exhibits a greater hike in the temperature field irrespective to the variation of other characterizing factors.
- The enhanced reacting species and the Lewis number show a substantial deceleration in the solutal bounding surface thickness due to decreasing solutal diffusivity.
- Solutal Peclet number and the bioconvection Lewis number give rise to retards the motile microorganism distribution and that resulted in a noteworthy deceleration in the profile thickness.
- The increasing shear rate and the resistivity due to the implementation of the permeability enhances the shear rate but both the buoyancy forces retard the shear rate profile.

- The heat transfer rate attenuates for the increasing thermal radiation but the solutal transfer rate enhances for the enhanced Lewis number.

The proposed study neither shows the parametric analysis of the several factors on the flow phenomena but also reveals several recent applications. The study is useful in designing advanced bioreactors where the role of thermophoretic deposition of the solid particles play an important in improving microbial growth. Also applicable in modelling nanofluid based cooling systems for hyperthermia treatment. However, the study informs strategic role in improving heat transfer efficiency in industrial processes involving mixed convection. Moreover, in future the combined effect of bioconvection and thermal radiation may help to the development of more efficient drug delivery systems.

Author contribution All the authors have equally contributed to complete the manuscript, i.e. RB has formulated the problem and FO verified the problem statement, TMA has completed the draft with results and discussion section and SRM and SP checked the overall.

Data availability No datasets were generated or analysed during the current study.

Declarations

Conflict of interest The authors declare no competing interests.

References

Abbas M, Alotaibi H, Muhammad T, Ghazi HM (2024) A computational framework to explore the impact of heat generation and activation energy on Marangoni convective stagnation point flow of ternary hybrid nanofluid. Adv Mech Eng 16(12):16878132241304602

Abd El-Aziz M (2009) Viscous dissipation effect on mixed convection flow of a micropolar fluid over an exponentially stretching sheet. Can J Phys 87(4):359–368

Aboel-Magd Y, Basem A, Farooq U, Fatima N, Noreen S, Waqas H, Iftikhar M (2024) Computational modeling of thermal radiation and activation energy effects in casson nanofluid flow with bioconvection and microorganisms over a disk. Int J Thermofluids 23:100735

Agarwal P, Jain R, Loganathan K (2024) Thermally radiative flow of MHD Powell-Eyring nanofluid over an exponential stretching sheet with swimming microorganisms and viscous dissipation: a numerical computation. Int J Thermofluids 23:100773

Alghamdi M, Wakif A, Thumma T, Khan U, Baleanu D, Rasool G (2021) Significance of variability in magnetic field strength and heat source on the radiative-convective motion of sodium alginate-based nanofluid within a Darcy-Brinkman porous structure bounded vertically by an irregular slender surface. Case Stud Therm Eng 28:101428

Alharbi KAM, Farooq U, Waqas H, Imran M, Noreen S, Akgül A, Abbas K (2023) Numerical solution of Maxwell-Sutterby nanofluid flow inside a stretching sheet with thermal radiation, exponential heat source/sink, and bioconvection. Int J Thermofluids 18:100339

Amjad M, Khan MN, Ahmed K, Ahmed I, Akbar T, Eldin SM (2023) Magnetohydrodynamics tangent hyperbolic nanofluid flow over an exponentially stretching sheet: Numerical investigation. Case Stud Therm Eng 45:102900

Baithalu R, Mishra SR, Panda S (2024) Magnetic dissipation on radiative free convection of a conducting hybrid nanofluid within a rotating cone and circular disc. Part Differ Equat Appl Math 11:100788

Bellman RE, Kalaba RE (1965) Quasilinearization and nonlinear boundary-value problems, Modern analytic and computational methods in science and mathematics, Elsevier

Bidin B, Nazar R (2009) Numerical solution of the boundary layer flow over an exponentially stretching sheet with thermal radiation. Eur J Sci Res 33(4):710–717

Choudhary P, Choudhary S, Jat K, Loganathan K, Eswaramoorthi S (2024) Significances of Melting Heat Transfer and Bioconvection Phenomena in Nanofluid Flow over three different geometries. Int J Thermofluids 24:100855

Chu YM, Ibrahim M, Saeed T, Berrouk AS, Algehyne EA, Kalbasi R (2021) Examining rheological behavior of MWCNT-TiO2/5W40 hybrid nanofluid based on experiments and RSM/ANN modeling. J Mol Liq 333:115969

Das T, Mkhatshwa MP, Gope R, Mondal S (2023) Analyses of entropy generation in micropolar liquid using overlapping multi-domain spectral quasilinearization method. Heliyon 9(3):e14432

Elboughdiri N, Abbas M, Ayed H, Mouldi A, Fatima N, Abduvalieva D, Galal AM (2024) Numerical simulation of stephan blowing impacts on thermally laminated 3D flow of MHD trihybrid nanofluid with soret and dufour effects. Case Stud Therm Eng 105460

Faizan M, Zafar SS, Ali F, Lone SA, Saeed A (2024) Modeling of magneto bioconvection Williamson nanoliquid through modified heat flux: the significance of entropy. Partial Different Equat Appl Math 10:100746

Francis P, Sambath P, Fernandez-Gamiz U, Noeiaghdam S, Dinarvand S (2024) Computational analysis of bio-convective eyring-powell nanofluid flow with magneto-hydrodynamic effects over an isothermal cone surface with convective boundary condition. Heliyon 10(3):e25088

Fuzhang W, Anwar MI, Al, M, El-Shafay AS, Abbas N, Ali R (2022) Inspections of unsteady micropolar nanofluid model over exponentially stretching curved surface with chemical reaction. Waves in random and complex media, 1–22

Hsiao KL (2017) Micropolar nanofluid flow with MHD and viscous dissipation effects towards a stretching sheet with multimedia feature. Int J Heat Mass Transf 112:983–990

Ishak A (2011) MHD boundary layer flow due to an exponentially stretching sheet with radiation effect. Sains Malaysiana 40(4):391–395

Janapatla P, Chakraborty A (2023) Mixed convection nanofluid flow using lie group scaling with the impact of mhd, radiation, thermophoresis and brownian motion over a vertical wedge. J Adv Res Fluid Mech Therm Sci 101(2):85–98

Kumar A, Tripathi R, Singh R, Chaurasiya VK (2020) Simultaneous effects of nonlinear thermal radiation and Joule heating on the flow of Williamson nanofluid with entropy generation. Physica A 551:123972

Layek GC, Mukhopadhyay S, Samad SA (2007) Heat and mass transfer analysis for boundary layer stagnation-point flow towards a heated porous stretching sheet with heat absorption/generation and suction/blowing. Int Commun Heat Mass Transfer 34(3):347–356

Li Y, Mishra SR, Pattnaik PK, Baag S, Li Y, Khan MI, Khan NB, Alaoui MK, Khan SU (2022) Numerical treatment of time dependent magnetohydrodynamic nanofluid flow of mass and heat transport subject to chemical reaction and heat source. Alexandria Eng J 61:2484–2491. https://doi.org/10.1016/j.aej.2021.07.030

Loganathan K, Rajan S (2020) An entropy approach of Williamson nanofluid flow with Joule heating and zero nanoparticle mass flux. J Therm Anal Calorim 141(6):2599–2612

Magyari E, Keller B (1999) Heat and mass transfer in the boundary layers on an exponentially stretching continuous surface. J Phys D Appl Phys 32(5):577

Mahariq I, Abbas M, Fatima N, Akgül A, Faqihi AA (2025) Significance of melting phenomena on Darcy-Forchheimer flow of trihybrid nanofluid over a disk in the presence of thermophoresis particles deposition. Multiscale Multidisciplin Model Experim Design 8(1):1–17

Mahmud K, Rana S, Al-Zubaidi A, Mehmood R, Saleem S (2022) Interaction of Lorentz force with cross swimming microbes in couple stress nano fluid past a porous Riga plate. Int Commun Heat Mass Transfer 138:106347. https://doi.org/10.1016/j.icheatmasstransfer.2022.106347

Motsa SS (2013) A new spectral local linearization method for nonlinear boundary layer flow problems. J Appl Math 2013(1):423628

Mukhopadhyay S, Gorla RSR (2012) Effects of partial slip on boundary layer flow past a permeable exponential stretching sheet in presence of thermal radiation. Heat Mass Transf 48:1773–1781

Okasha MM, Abbas M, Formanova S, Faiz Z, Ali AH, Akgül A, Galal AM (2024) Scrutinization of local thermal non-equilibrium effects on stagnation point flow of hybrid nanofluid containing gyrotactic microorganisms: a bio-fuel cells and bio-microsystem technology application. J Therm Analy Calorim 1–15

Prasannakumara BC, Madhukesh JK, Ramesh GK (2023) Bioconvective nanofluid flow over an exponential stretched sheet with thermophoretic particle deposition. Propuls Power Res 12(2):284–296

Ratha PK, Mishra SR, Tripathy RS (2022) Exploration of dissipative heat energy in conjunction with various thermophysical properties of nanofluids: Water and ethylene glycol base fluids. Int Commun Heat Mass Transfer. 138:106423. https://doi.org/10.1016/j.icheatmasstransfer.2022.106423

Rehman MIU, Chen H, Khan MI, Hamid A, Masmoudi A (2024) Modeling and predicting heat transfer performance in bioconvection flow around a circular cylinder using an artificial neural network approach. Tribol Int 200:110182

Thumma T, Mishra SR, Abbas MA, Bhatti MM, Abdelsalam SI (2022) Three-dimensional nanofluid stirring with non-uniform heat source/sink through an elongated sheet. Appl Math Comput 421:126927. https://doi.org/10.1016/j.amc.2022.126927

Ullah I, Khan WA, Jamshed W, Abd-Elmonem A, Abdalla NSE, Ibrahim RW, ElSeabee FAA (2023) Heat generation (absorption) in 3D bioconvection flow of Casson nanofluid via a convective heated stretchable surface. J Mol Liquids 392:123503

Wang F, Rehman S, Shah MH, El Yamani MA, Farooq S, Farooq A (2025) Numerical computation of cross nanofluid model using neural network and Adaptive Neuro-Fuzzy Inference system with statistical insights for enhanced flow optimization. Expert Syst Appl 263:125721

Wang F, Parveen R, Rehman S, Farooq A, Alhazmi H, Aljohani AF, Omer AS (2024) Artificial neural computing and statistical analysis of heat and mass transport of nanofluid flow with melting heat and thermal stratification. Case Stud Therm Eng 104563

Waseem M, Jawad M, Naeem S, Bognár G, Alballa T, Khalifa HAEW, Kolsi L (2024) Regression analysis of Cattaneo-Christov heat and thermal radiation on 3D Darcy flow of Non-Newtonian fluids induced by stretchable sheet. Case Stud Therm Eng 61:104959

Publisher's Note Springer Nature remains neutral with regard to jurisdictional claims in published maps and institutional affiliations.

Springer Nature or its licensor (e.g. a society or other partner) holds exclusive rights to this article under a publishing agreement with the author(s) or other rightsholder(s); author self-archiving of the accepted manuscript version of this article is solely governed by the terms of such publishing agreement and applicable law.